Ultrafast triggering of insulator-metal transition in two-dimensional VSe_2

Deepnarayan Biswas,[†] Alfred J. H. Jones,[†] Paulina Majchrzak,[†,‡] Byoung Ki Choi,[¶] Tsung-Han Lee,[§] Klara Volckaert,[†] Jiagui Feng,[‖,⊥] Igor Marković,[‖,#] Federico Andreatta,[†] Chang-Jong Kang,[§] Hyuk Jin Kim,[¶] In Hak Lee,[¶] Chris Jozwiak,[@] Eli Rotenberg,[@] Aaron Bostwick,[@] Charlotte E. Sanders,[‡] Yu Zhang,[‡] Gabriel Karras,[‡] Richard T. Chapman,[‡] Adam S. Wyatt,[‡] Emma Springate,[‡] Jill A. Miwa,[†] Philip Hofmann,[†] Phil D. C. King,[‖] Young Jun Chang,[¶,△] Nicola Lanata,[†,●] and Søren Ulstrup*[,†]

†*Department of Physics and Astronomy, Interdisciplinary Nanoscience Center, Aarhus University, 8000 Aarhus C, Denmark*

‡*Central Laser Facility, STFC Rutherford Appleton Laboratory, Harwell 0X11 0QX, UK*

¶*Department of Physics, University of Seoul, Seoul 02504, Republic of Korea*

§*Department of Physics and Astronomy, Rutgers University, Piscataway, NJ 08856, USA*

‖*SUPA, School of Physics and Astronomy, University of St Andrews, St Andrews KY16 9SS, UK*

⊥*Suzhou Institute of Nano-Tech. and Nanobionics (SINANO),CAS, 398 Ruoshui Road, SEID, SIP, Suzhou, 215123, China*

#*Max Planck Institute for Chemical Physics of Solids, Nöthnitzer Straße 40, 01187 Dresden, Germany*

@*Advanced Light Source, E. O. Lawrence Berkeley National Laboratory, Berkeley, CA 94720, USA*

△*Department of Smart Cities, University of Seoul, Seoul, 02504, Republic of Korea*

●*Nordita, KTH Royal Institute of Technology and Stockholm University, Roslagstullsbacken 23, 10691 Stockholm, Sweden*

Abstract

The transition metal dichalcogenide VSe_2 exhibits an increased charge density wave transition temperature and an emerging insulating phase when thinned to a single layer. Here, we investigate the interplay of electronic and lattice degrees of freedom that underpin these phases in single-layer VSe_2 using ultrafast pump-probe photoemission spectroscopy. In the insulating state, we observe a light-induced closure of the energy gap, which we disentangle from the ensuing hot carrier dynamics by fitting a model spectral function to the time-dependent photoemission intensity. This procedure leads to an estimated timescale of 480 fs for the closure of the gap, which suggests that the phase transition in single-layer VSe_2 is driven by electron-lattice interactions rather than by Mott-like electronic effects. The ultrafast optical switching of these interactions in SL VSe_2 demonstrates the potential for controlling phase transitions in 2D materials with light.

KEYWORDS: Single-layer VSe_2, metal-insulator transition, charge density wave, ultrafast dynamics, time- and angle-resolved photoemission spectroscopy.

Assembling transition metal dichalcogenides (TMDCs) at the two-dimensional (2D) limit is a promising approach for tailoring emerging states of matter such as superconductivity or charge density waves (CDWs).[1–5] Single-layer (SL) VSe_2 stands out in this regard because it exhibits a strongly enhanced CDW transition with a higher critical temperature compared to the bulk in addition to an insulating phase with an anisotropic gap at the Fermi level,[6–10] causing a suppression of anticipated 2D ferromagnetism in the material.[7,11–14] The CDW is linked to strong Fermi surface nesting, which leads to a gap around the nested segments of the electronic band structure that has been reported to persist to temperatures of 220 K[8] and 350 K.[6] The insulating phase emerges at a transition temperature of 135 K and is accompanied by $(\sqrt{3}\times 2)$ and $(\sqrt{3}\times\sqrt{7})$ lattice distortions.[6–8,14] The role of the electron and lattice degrees of freedom underpinning this phase remains controversial.[6–8,10,11,13,14]

Employing an ultrafast laser pulse to optically excite SL VSe_2 in a time- and angle-

resolved photoemission spectroscopy (TR-ARPES) experiment gives access to the energy-, momentum- and time-dependent response of the material and thereby the transient electronic band structure and many-body interactions. Similar experiments on bulk TMDCs have revealed the timescales for melting CDW and Mott insulator phases[15–19] and provided Cooper pair recombination rates in high-temperature superconductors.[20,21] The timescales on which the electronic system evolves following excitation lead to detailed insights into the hierarchy of interactions underpinning the phase transition. For example, electronic degrees of freedom typically respond on timescales in the range of $10 - 100$ fs.[16,22] Processes driven by lattice degrees of freedom occur on timescales on the order of 100 fs if they involve coherent phonon excitations, whereas incoherent electron-phonon scattering is usually significantly slower than the corresponding amplitude mode oscillations.[22–24]

We focus on the insulating phase in SL VSe_2 grown by molecular beam epitaxy on bilayer (BL) graphene on silicon carbide.[6,7] Before discussing the response of the system to an optical excitation, we start by clarifying the electronic structure of the material and characterize the temperature dependence of the phase transition in static conditions. Above the critical temperature T_c, the material assumes the 1T structural modification where the V and Se atoms are coordinated in an octahedral geometry as shown in Fig. 1(a). The dispersion of this phase is calculated using density functional theory (DFT) and presented together with an ARPES spectrum along the high symmetry $\bar{\text{M}}$-$\bar{\Gamma}$-$\bar{\text{K}}$ direction in Fig. 1(b). The shallow states around E_F are composed of V $3d$ orbitals while the dispersive subbands at higher binding energies derive from Se $4p$ orbitals (see Supplementary Fig. S1). The increased broadening of V $3d$ states with energy below E_F and the enhanced effective masses compared to the DFT dispersion are the telltale signs of correlation effects. Indeed, we find that these effects are captured in our dynamical mean-field theory (DMFT) calculations for a relatively large Hubbard interaction strength U as shown in Fig. 1(c) for $U = 6$ eV (see also Supplementary Fig. S2).

In order to deconvolve single-particle and many-body effects from the ARPES spec-

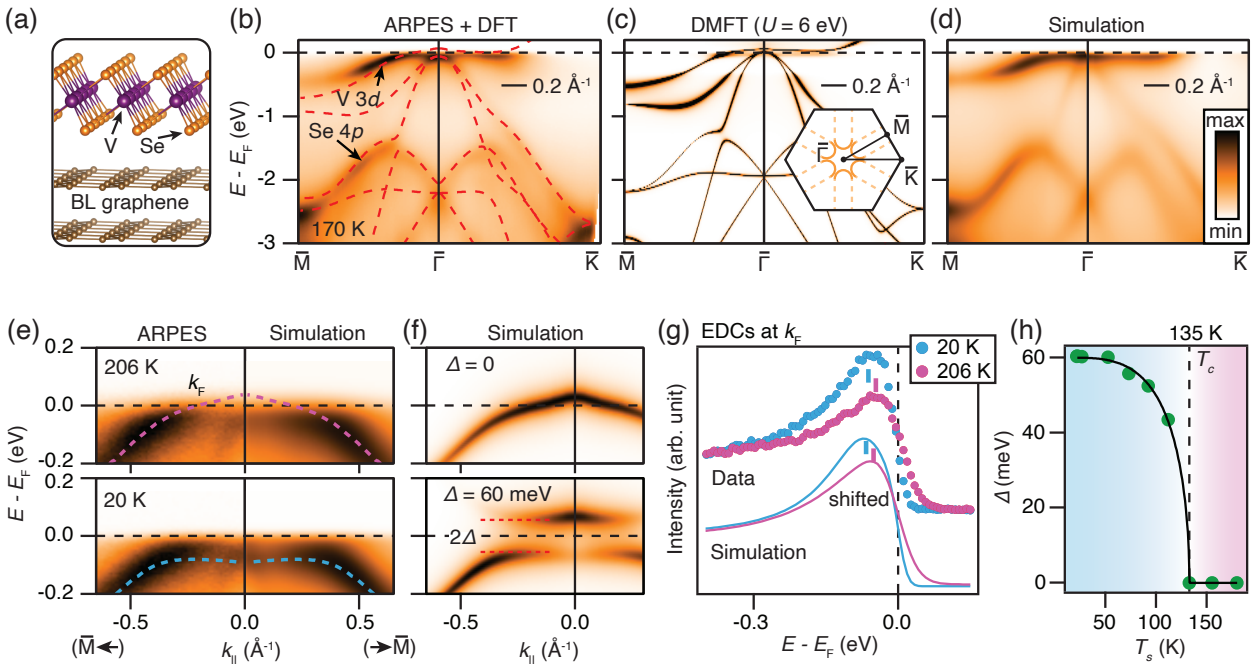

Figure 1: Electronic structure and temperature dependent phase transition in SL VSe_2. (a) Schematic of 1T structure of SL VSe_2. (b) ARPES data collected at 170 K in the $\bar{M}$-$\bar{\Gamma}$-$\bar{K}$ direction. The dashed red lines correspond to the calculated DFT dispersion (the raw data without DFT bands is shown in Supplementary Fig. S3). (c) DMFT spectrum for U = 6 eV. The inset presents the SL VSe_2 BZ with contours sketching the Fermi surface at 170 K. (d) Numerical simulation of the 2D ARPES intensity optimized to the data in (b). (e) ARPES spectra and corresponding simulation along $\bar{M}$-$\bar{\Gamma}$ for the given sample temperatures (see Supplementary Video 1 and Supplementary Fig. S3). The dashed lines represent the simulated dispersion including many-body effects. (f) Simulation of photoemission intensity with the Fermi-Dirac function removed for the given values of the gap parameter Δ. (g) Comparison of EDCs at k_F for sample temperatures of 206 and 20 K. The cuts were obtained from the data (markers) and simulation (curves) in (e). Tick marks indicate EDC peak positions, demonstrating a shift away from E_F with decreasing sample temperature. (h) Extracted values (markers) of Δ from spectra obtained at several sample temperatures along with a fit (black curve) to a mean-field expression describing the phase transition. The fitted value of T_c is shown via a dashed vertical line.

tra we are following the phenomenological model of the photoemission intensity, $\mathcal{I}(k,\omega) = |\mathcal{M}(k,\omega)|^2 \mathcal{A}(k,\omega) n_{\mathrm{FD}}(\omega)$.[25] Here, $\mathcal{A}(k,\omega)$ is the spectral function, $\mathcal{M}(k,\omega)$ incorporates the single-electron dipole matrix elements that govern the selection rules of the photoemission process and $n_{\mathrm{FD}} = (e^{(\omega-\mu)/k_B T_e} + 1)^{-1}$ is the Fermi-Dirac (FD) distribution function with chemical potential μ and electronic temperature T_e. By combining the bare dispersion

obtained from DFT with the electronic self-energy, Σ, deduced from the DFT and LDA + DMFT calculation, we are able to construct the spectral function of SL VSe_2, as described in further details in the Methods. A numerical simulation of $\mathcal{I}(k,\omega)$ with self-energy and matrix elements adjusted to give an optimum description of the measured 2D image of the photoemission intensity is shown in Fig. 1(d), providing a basic model to interpret ARPES spectra of SL VSe_2 in the following discussion.

We focus on measurements along the $\bar{\text{M}}$-$\bar{\Gamma}$ high symmetry direction in order to track the opening of a gap in the Fermi surface segment shown in the Brillouin zone (BZ) sketch in Fig. 1(c), which occurs when the sample is cooled below T_c.[6,10] A detailed view of this cut is presented for sample temperatures T_s of 206 and 20 K around the Fermi crossing k_{F} in Fig. 1(e). A significant T_s-dependent change of the V $3d$ dispersion is seen via the purple and blue dashed curves that have been extracted using our 2D simulation of the intensity (see transition in Supplementary Video 1). The change of dispersion is linked to the gap opening described in terms of the parameter Δ, which is demonstrated in the simulation with the FD function removed in Fig. 1(f). For $\Delta = 0$ the band crosses E_{F}, however, the intensity around the band maximum is not seen in the ARPES data because these states are unoccupied. As Δ assumes a finite value, a gap of 2Δ opens, leading to increased spectral weight around $\bar{\Gamma}$ below E_{F}. The presence of such a gap is further corroborated by a shift of the peak away from E_{F} in energy distribution curve (EDC) cuts at k_{F} as T_s is lowered, which is demonstrated in Fig. 1(g). The complete T_s-dependence of Δ is determined by fitting the 2D ARPES intensity measured at several temperatures, leading to the phase diagram in Fig. 1(h). The critical temperature found using this method is 135 ± 5 K, which is consistent with previous studies.[6,7]

On the basis of the spectroscopic signatures and modeling of the insulator-metal transition specified above, we are now able to analyze the time-dependent response of SL VSe_2 to an optical excitation. Measurements performed with sample temperatures of 200 K and 88 K are compared in order to track the dynamics in both the metallic and insulating phases.

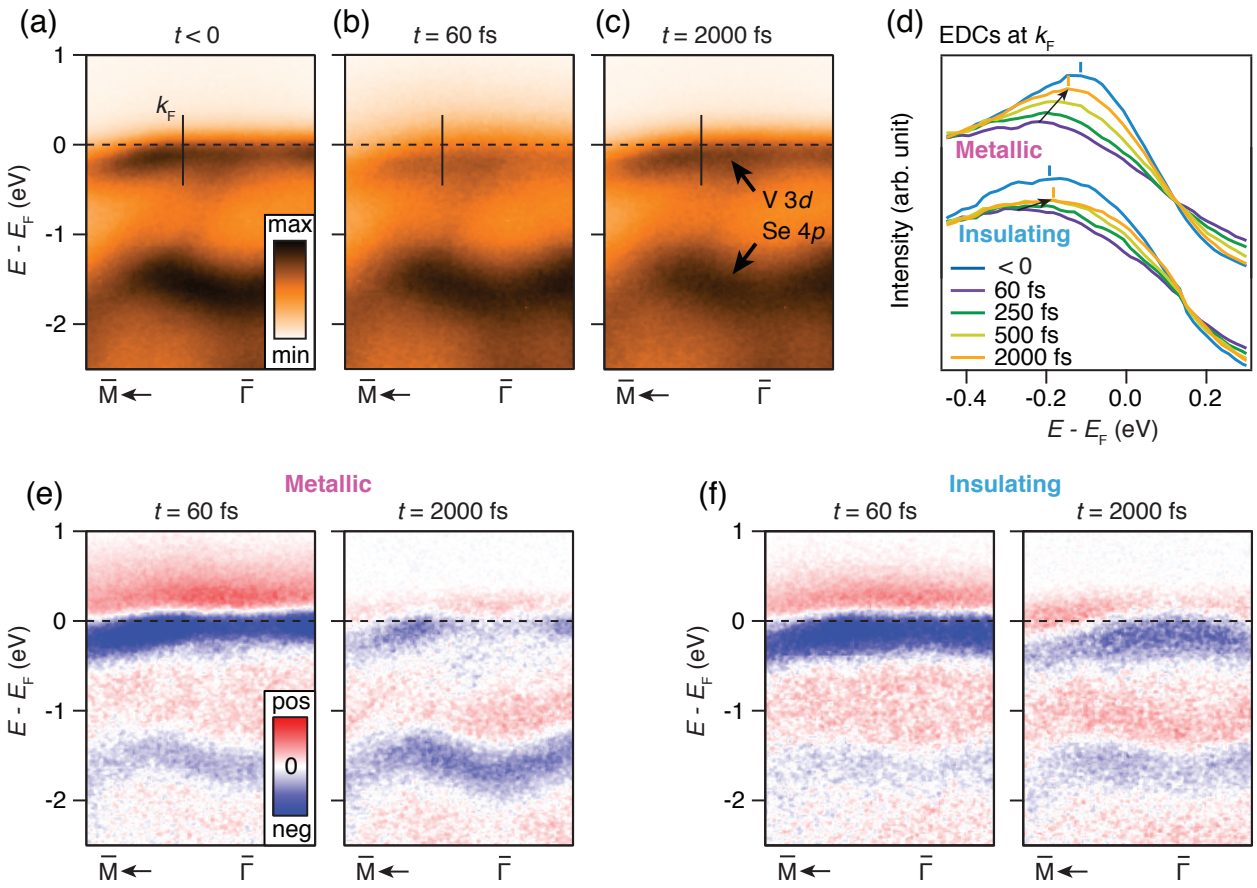

Figure 2: Optical excitation of SL VSe_2. (a)-(c) ARPES spectra of V 3d and Se 4p bands (see arrows in (c)) revealing the response of the electronic structure (a) before (t < 0), (b) at the peak (t = 60 fs) and (c) at a long delay (t = 2000 fs) after optical excitation. All spectra are obtained along the $\bar{M}$-$\bar{\Gamma}$ direction and with the sample temperature initially at 200 K. (d) EDCs extracted along the vertical line at k_F shown in (a)-(c) for the stated time delays for both the metallic phase and the insulating phase. The blue and orange tick marks represent peak positions for the curves at t < 0 and t = 2000 fs and the black arrows illustrates the change in peak position from 60 to 2000 fs, resulting from a polynomial fit around each peak. (e) Intensity difference for the metallic phase obtained by subtracting the equilibrium spectrum in (a) from the excited state spectra at the given time delays in (b)-(c). (f) Similar difference spectra as shown in (e) measured for the insulating phase.

TR-ARPES snapshots are shown along $\bar{M}$-$\bar{\Gamma}$ in Figs. 2(a)-(c) for excitation of the metallic phase using a pump pulse with an energy of 1.56 eV and a fluence around 5 mJ/cm^2 at a time delay t before the optical excitation (t < 0), at the peak of the excitation (t = 60 fs) and at a longer delay (t = 2000 fs). The overall time-resolution of the experiment is 54 fs. The excitation leads to a substantial decrease in intensity in the V 3d states around E_F (see panel (b)),

which does not fully recover at longer delays (see panel (c)). The raw (ω, k, t)-dependent intensity measured under the same conditions for the insulating phase appears similar on a superficial view (see Supplementary Fig. S3 for a comparison). Significant changes in the optical response of the two phases are visible when inspecting raw EDCs extracted for a series of time delays around k_{F}, as shown in Fig. 2(d). In both phases, the optical excitation initially leads to a reduction of intensity and a peak shift towards higher binding energies. However, in the metallic phase, the intensity and peak position gradually approach the equilibrium situation, as indicated by a black arrow in the top curves of panel (d). This behavior merely reflects the changing width of the FD distribution due to the temperature dependence of the electronic temperature T_e, as observed in other metallic systems.[23,26] In the insulating phase, the EDC intensity and peak position do not gradually shift towards the equilibrium value. From 500 to 2000 fs the peak intensity remains strongly reduced, as indicated by a black arrow, and at 2000 fs the peak has shifted closer to E_{F} compared to the equilibrium peak position, as seen via the blue and orange tick marks above the bottom set of curves in panel (d). This behavior is indicative of a gap closing effect, similarly as shown in Fig. 1(g).

A stronger indication for the spectral changes following excitation is obtained by calculating the difference in photoemission intensity by subtracting a spectrum determined in equilibrium conditions before the arrival of the pump pulse from the spectrum measured at a given delay time as shown for the two phases in Figs. 2(e)-(f) and Supplementary Video 2. A highly complex ω- and k-dependence of intensity depletion and increase is seen. Surprisingly, we observe strong difference signals persisting at long delays (t = 2000 fs) that look dramatically different close to $\bar{\Gamma}$ and E_F for the two phases. Naively, one could think of assigning these changes to the mere redistribution of charge carriers in the V $3d$ and Se $4p$ states with excited holes (electrons) signified by the blue (red) regions of the spectra. However, the intensity is simultaneously affected by a change of the FD distribution due to the elevated electronic temperature T_e, a t-dependence of the quasiparticle scattering rate

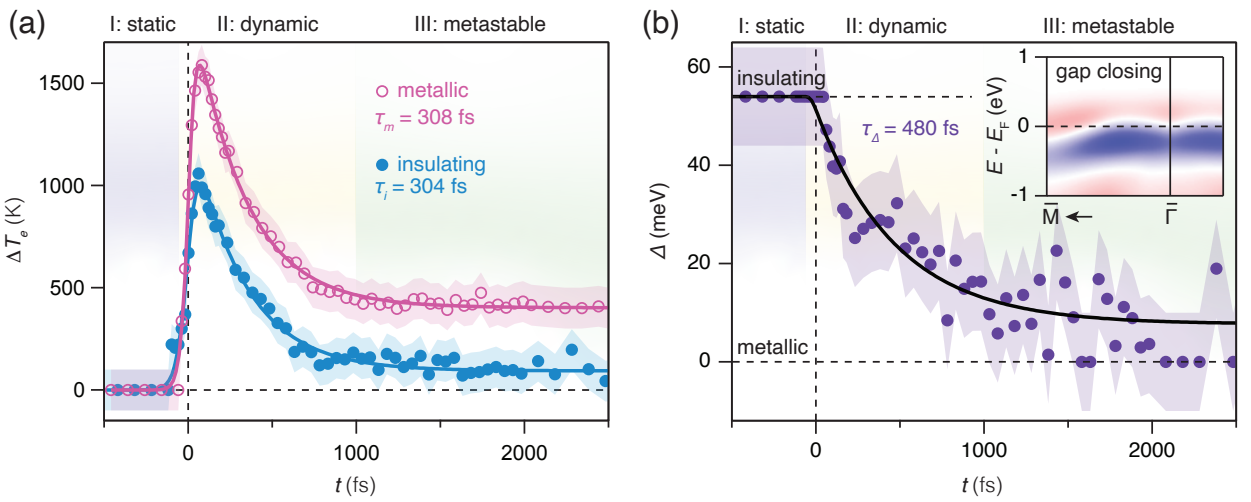

Figure 3: Dynamics of hot carriers and phase transition. (a) Time-dependent change of electronic temperature determined by fitting the full (ω, k)-dependence of the photoemission intensity at each measured time delay in the metallic (open purple circles) and insulating (filled blue circles) phases. The full curves are fits to a function consisting of an exponential rise followed by an exponential decay with the given time constants $\tau_{\mathrm{m(i)}}$ for the decay in the metallic (insulating) phase. The shaded areas correspond to three distinct periods of the time-dependent response labeled as (I) static, (II) dynamic and (III) metastable. (b) Time-dependence of Δ. The solid curve is a fit to an exponential decay with a time constant of τ_Δ = 480 fs. The inset presents the intensity difference between a fitted spectrum for the insulating state at equilibrium and a spectrum for the metastable metallic state, incorporating a change of Δ from 54 meV to zero. The shaded regions around the data points in (a)-(b) represent the uncertainity associated with the analysis.

Γ that manifests itself as increased broadening of the bands,[26,27] and the possibility of a t-dependent Δ in the insulating phase. Using our model of the photoemission intensity presented in Fig. 1(d) we fit T_e, Γ and Δ such that our simulated intensity gives an optimum description of the ARPES intensity at all measured time delays, noting that Δ = 0 for the metallic phase (see Methods and Supplementary Section 3 for further details of the fit). An excellent fit is obtained for all time delays in both phases using our assumption of a hot carrier model where the simulated intensity always incorporates a well-defined FD function, indicating that thermalization occurs via electron-electron interactions on a faster timescale than we can resolve (< 40 fs).[28]

The change of electronic temperature extracted from this analysis is presented in Fig.

3(a), revealing a qualitatively similar t-dependence in the two phases that can be divided according to (I) a static period before excitation, (II) a dynamic period with a sharp rise of T_e during excitation followed by an initial fast relaxation and (III) a metastable period where the system remains out of equilibrium and does not relax on the timescale of our measurement. The transient increase in electronic temperature is caused by ultrafast energy transfer from the laser pulse to the electrons in the V $3d$ states. Energy is then transferred from electrons to strongly coupled lattice vibrations, leading to a decay of T_e on a timescale of ≈300 fs. Both insulating and metallic phases subsequently reach a stable elevated electronic temperature compared to equilibrium with a temperature larger than T_c.

Figure 3(b) presents the extracted t-dependence of Δ from the TR-ARPES measurement of the insulating phase, revealing a transient closure of the gap during the dynamic period (region II) with a time constant determined to be τ_Δ = 480 fs from an exponential fit, leaving the system in a metastable metallic phase (region III). The intensity difference between the fitted spectrum in this metastable metallic state and the insulating state in equilibrium (region I) essentially reproduces the measured behavior, as seen by comparing the inset in Fig. 3(b) with the difference spectrum at t = 2000 fs in Fig. 2(f) (see Supplementary Fig. S5 for other fit parameters and fitted difference spectra in the metallic phase). The change in Δ is essential for the simulation of this distinct redistribution of intensity as demonstrated in Supplementary Fig. S6, and it is highly reproducible over multiple samples as shown in Supplementary Fig. S7. It is important to stress that a change of Δ on the scale of a few tens of meV does not translate into a change of the photoemission intensity on the same small energy scale, as this would indeed be challenging to resolve with the energy resolution of our TR-ARPES experiment. Rather, the change in Δ affects the shape of the spectral function of SL VSe_2 via the band dispersion and linewidth of the entire V $3d$ band, which is what we can reliably extract using our 2D analysis of the (ω, k)-dependent intensity at each time delay. We note that future TR-ARPES experiments with high energy resolution would be required to directly resolve the gap closing effect, in addition to the spectral function

changes over the wider energy range we observe here.

The insulating gap melting time, τ_Δ = 480 fs, should be viewed as an estimate based on our spectral function analysis. We note that there are substantial error bars associated with this value, as can be seen in Fig. 3(b). However, combining τ_Δ with the associated thermal relaxation timescale of ≈300 fs that describes the decay of hot electrons in Fig. 3(a) we can generally conclude that the dynamics of the insulator-metal transition occurs on the timescale of several hundreds of femtoseconds. This excludes a Mott transition, because processes driven by electron-electron interactions occur on a timescale that is an order of magnitude faster.[22] This is an important interaction to exclude given the large Hubbard U value determined for the V $3d$ states, which points towards significant electronic correlations in the system. Instead, there are two important scenarios based on electron-lattice interactions to consider. The first involves a Peierls transition where photodoping lifts the periodic ($\sqrt{3} \times 2$) and ($\sqrt{3} \times \sqrt{7}$) lattice distortions. The timescale in such a process is a quarter period of the relevant amplitude mode,[15–19] which has been measured using Raman spectroscopy in bulk VSe_2 to be around 130 fs, considering the E_g mode.[29] The estimated τ_Δ is too slow for such processes as well. This strongly suggests that the dynamics is driven by incoherent energy transfer from the hot electrons to a few strongly coupled phonons. This scenario can be understood within the framework of a three-temperature model (3TM) where a distribution of high energy optical phonons, likely involving the strongly coupled E_g mode,[29] constitutes the main efficient relaxation channel for the hot electrons.[30] Anharmonic decay of such strongly coupled phonons on a timescale that is comparable to the gap melting time of 480 fs leads to thermalization with the remaining lattice at a temperature above T_c in the metastable state. The appearance of this metastable state is strongly indicative of a slow reconfiguration of the thermally excited lattice, leaving the system in a stable configuration in the metallic state with an energy barrier separating it from the insulating state, similarly as observed for metal-insulator transitions in a range of other materials.[31–34] The melting of the insulating gap does not lead to a long-range magnetic ordering,[11] as this would lead to a

splitting of the electronic states into minority and majority carrier bands[7] - a scenario which we can clearly rule out from the TR-ARPES spectra measured after the optical excitation. The detailed lattice dynamics and the possibility of local ferromagnetic fluctuations in SL VSe_2 may be resolved in future studies utilizing ultrafast probes of the lattice structure.

In conclusion, we have tracked the spectral function of SL VSe_2 across an ultrafast insulator-metal transition triggered by an intense optical excitation. The spectroscopic signatures of hot carrier dynamics and phase transition could be disentangled, revealing that electron-lattice energy exchange drives the transition in the first few hundreds of femtoseconds following excitation and leads to a metastable metallic state. Such a situation is not only intriguing for the application of 2D materials in electronic memory devices, but the coupling between electron and lattice degrees of freedom is also of fundamental interest for understanding the interplay of CDW physics and magnetism in 2D.

Methods

Sample preparation. SL VSe_2 samples were grown on BL graphene on 6H-SiC(0001) using molecular beam epitaxy (MBE) at a base pressure better than $2 \cdot 10^{-10}$ Torr. The sample measured to produce the data in Fig. 1(b) was grown at the University of St Andrews, UK. The remaining spectra were collected on samples grown at the University of Seoul, Republic of Korea. Details of the growth parameters and the RHEED data are available in Supplemental section 5.[35,36] After growth, the sample was annealed at 450 °C for 30 min. A 100 nm Se film was deposited at room temperature to protect the sample while transferring through air. This Se capping layer was removed by annealing the sample at 300 °C for several hours in the UHV analysis chamber before photoemission experiments. No noticeable change in sample quality was observed due to the capping and de-capping procedure.

ARPES experiments. The static ARPES spectrum shown in Fig. 1(b) was collected

using a high-intensity He lamp ($h\nu$ = 21.2 eV, p-polarization) and a SPECS Phoibos 225 hemispherical electron analyzer at University of St Andrews, UK. Here, samples were directly transferred from the attached MBE growth chamber to the ARPES chamber. The remaining static measurements were performed in the microARPES end-station (base pressure of $\sim 3 \cdot 10^{-11}$ Torr) at the MAESTRO facility at beamline 7.0.2 of the Advanced Light Source, Lawrence Berkeley National Laboratory. The ARPES system was equipped with a Scienta R4000 electron analyzer. We used a photon energy of 48 eV for T_s-dependent scans. The total energy and angular resolution of our experiments were better than 20 meV and 0.1°, respectively.

The Materials Science end station of the Artemis facility at Rutherford Appleton Laboratory was used for TR-ARPES measurements. Synchronized infrared (IR) pump and extreme ultraviolet (EUV) probe beams were generated from a Ti:Sapphire laser system at 12 mJ, 1 kHz, with a 30 fs pulse length and a central wavelength of 795 nm. A small fraction of the energy was used directly to pump the sample at 1.56 eV. The remaining laser intensity was focused into a thin Ar gas cell to generate a comb of odd harmonics in the EUV. The 19th harmonic at 29.6 eV was selected as the probe, using a time-preserving monochromator.[37] The pump beam was s-polarised while the probe beam was p-polarised. The end station was equipped with a SPECS Phoibos 100 hemispherical electron energy analyser. The time, energy and angular resolution of our measurements were 54 fs (Supplementary section 6), 250 meV and 0.3° respectively. Temperatures from 88 to 220 K were reached using an open-cycle liquid He cryostat.

Theory and simulations. The LDA+DMFT calculations were performed at a temperature of T_s = 200 K, assuming a Hund's rule coupling J = 0.8 eV and scanning different values of the screened Hubbard interaction strength U from 5 to 9 eV. We utilized the DMFT package of Ref. 38 for the electronic structure calculations interfaced with the local density approximation (LDA) functional implemented in Wien2k[39] and we adopted the

fully-localized-limit scheme for the double-counting functional.[40] All simulations have been performed with 10000 k-points and $Rkmax = 7$ and employing the continuous-time quantum Monte-Carlo (CTQMC) impurity solver.[41–43] The spectral properties were mapped onto the real axis using the maximum entropy method.[44] The DFT calculations were performed using a Perdew, Burke, and Ernzerhof (PBE) functional.[45]

For the photoemission intensity simulations described in the main text we use the following expression for the spectral function:[25,27,46]

$$\mathcal{A}_n(\boldsymbol{k},\omega) = -\frac{\pi^{-1}\Sigma''_n(\boldsymbol{k},\omega)}{\left(\omega - \epsilon_{\boldsymbol{k}n} - \Sigma'_n(\boldsymbol{k},\omega)\right)^2 + \Sigma''^2_n(\boldsymbol{k},\omega)}, \tag{1}$$

where $\epsilon_{\boldsymbol{k}n}$ is the non-interacting band dispersion or bare band, which we describe using the DFT dispersion as an input. The subscript n is the band index. Σ'_n and Σ''_n are the real and imaginary parts of the electronic self energy Σ_n, respectively. In our simulation the correlation effects in the V $3d$ states, including the gap opening of the dispersion, are included in Σ_n through the expression (see Supplementary Section 1 for further details)

$$\Sigma_n(\boldsymbol{k},\omega) = \Sigma_0 - \frac{1-Z}{Z}\omega - i\frac{\Gamma}{Z} + \frac{\Delta^2/Z}{\omega + Z(\epsilon_{\boldsymbol{k}n} + \Sigma_0) + i\Gamma_0}. \tag{2}$$

Here Σ_0 is a constant energy shift of the states, Z is the quasiparticle residue, Γ is quasiparticle scattering rate, Δ is the gap parameter and Γ_0 is a constant related to the change in the scattering rate due to the presence of a gap. We also used a parameter, labeled ΔE_s, to describe any rigid shift of E_{F} and the band energies. Such a shift may arise due to an external electric field associated with vacuum space charge or surface photo voltage.[47] Further details of the simulations are provided in Supplementary Section 3.

Acknowledgement

We thank Phil Rice, Alistair Cox and David Rose for technical support during the Artemis beamtime. We gratefully acknowledge funding from VILLUM FONDEN through the Young Investigator Program (Grant. No. 15375) and the Centre of Excellence for Dirac Materials (Grant. No. 11744), the Danish Council for Independent Research, Natural Sciences under the Sapere Aude program (Grant Nos. DFF-9064-00057B and DFF-6108-00409) and the Aarhus University Research Foundation. This work is also supported by National Research Foundation (NRF) grants funded by the Korean government (nos. NRF-2020R1A2C200373211 and 2019K1A3A7A09033389) and by the International Max Planck Research School for Chemistry and Physics of Quantum Materials (IMPRS-CPQM). The authors also acknowledge The Royal Society and The Leverhulme Trust. Access to the Artemis Facility was funded by STFC. The Advanced Light Source is supported by the Director, Office of Science, Office of Basic Energy Sciences, of the U.S. Department of Energy under Contract No. DE-AC02-05CH11231.

Supplementary Information

Supplementary Information and two Supplementary Videos are available free of charge via the internet at http://pubs.acs.org. The Supplementary Information contains 6 sections and 9 figures providing the derivation of the self-energy and the DMFT calculations for SL VSe_2, raw ARPES spectra for SL VSe_2 in metallic and insulating phases, detailed error analysis and parameters for the photoemission intensity fitting procedure, TR-ARPES data for other SL VSe_2 samples and at different sample temperatures, RHEED measurements during growth of VSe_2, and a determination of the TR-ARPES time-resolution. Supplementary Videos 1 and 2 present the temperature- and time-dependent evolution of the SL VSe_2 photoemission intensity, respectively.

Additional information

The authors declare that they have no competing financial interests.

Correspondence and requests for materials should be addressed to S. U. (ulstrup@phys.au.dk).

References

(1) Xi, X.; Zhao, L.; Wang, Z.; Berger, H.; Forró, L.; Shan, J.; Mak, K. Strongly enhanced charge-density-wave order in monolayer $NbSe_2$. *Nat. Nanotechnol.* **2015**, *10*, 765.

(2) Ugeda, M. et al. Characterization of collective ground states in single-layer $NbSe_2$. *Nat. Phys.* **2016**, *12*, 92.

(3) Sanders, C. E.; Dendzik, M.; Ngankeu, A. S.; Eich, A.; Bruix, A.; Bianchi, M.; Miwa, J. A.; Hammer, B.; Khajetoorians, A. A.; Hofmann, P. Crystalline and electronic structure of single-layer TaS_2. *Phys. Rev. B* **2016**, *94*, 081404.

(4) Pásztor, Á.; Scarfato, A.; Barreteau, C.; Giannini, E.; Renner, C. Dimensional crossover of the charge density wave transition in thin exfoliated VSe_2. *2D Mater.* **2017**, *4*, 041005.

(5) Chen, Y. et al. Strong correlations and orbital texture in single-layer 1T-$TaSe_2$. *Nature Physics* **2020**, *16*, 218–224.

(6) Duvjir, G. et al. Emergence of a Metal–Insulator Transition and High-Temperature Charge-Density Waves in VSe_2 at the Monolayer Limit. *Nano Lett.* **2018**, *18*, 5432–5438.

(7) Feng, J. et al. Electronic Structure and Enhanced Charge-Density Wave Order of Monolayer VSe_2. *Nano Lett.* **2018**, *18*, 4493–4499.

(8) Chen, P.; Pai, W. W.; Chan, Y.-H.; Madhavan, V.; Chou, M. Y.; Mo, S.-K.; Fedorov, A.-V.; Chiang, T.-C. Unique Gap Structure and Symmetry of the Charge Density Wave in Single-Layer VSe_2. *Phys. Rev. Lett.* **2018**, *121*, 196402.

(9) Strocov, V. N.; Shi, M.; Kobayashi, M.; Monney, C.; Wang, X.; Krempasky, J.; Schmitt, T.; Patthey, L.; Berger, H.; Blaha, P. Three-Dimensional Electron Realm in VSe_2 by Soft-X-Ray Photoelectron Spectroscopy: Origin of Charge-Density Waves. *Phys. Rev. Lett.* **2012**, *109*, 086401.

(10) Umemoto, Y.; Sugawara, K.; Nakata, Y.; Takahashi, T.; Sato, T. Pseudogap, Fermi arc, and Peierls-insulating phase induced by 3D–2D crossover in monolayer VSe_2. *Nano Res.* **2019**, *12*, 165–169.

(11) Fumega, A. O.; Gobbi, M.; Dreher, P.; Wan, W.; González-Orellana, C.; Peña-Díaz, M.; Rogero, C.; Herrero-Martín, J.; Gargiani, P.; Ilyn, M.; Ugeda, M. M.; Pardo, V.; Blanco-Canosa, S. Absence of Ferromagnetism in VSe_2 Caused by Its Charge Density Wave Phase. *The Journal of Physical Chemistry C* **2019**, *123*, 27802–27810.

(12) Bonilla, M.; Kolekar, S.; Ma, Y.; Diaz, H. C.; Kalappattil, V.; Das, R.; Eggers, T.; Gutierrez, H. R.; Phan, M.-H.; Batzill, M. Strong room-temperature ferromagnetism in VSe_2 monolayers on van der Waals substrates. *Nat. Nanotechnol.* **2018**, *13*, 289–293.

(13) Coelho, P. M.; Nguyen Cong, K.; Bonilla, M.; Kolekar, S.; Phan, M.-H.; Avila, J.; Asensio, M. C.; Oleynik, I. I.; Batzill, M. Charge Density Wave State Suppresses Ferromagnetic Ordering in VSe_2 Monolayers. *J. Phys. Chem. C* **2019**, *123*, 14089–14096.

(14) Wong, P. K. J. et al. Evidence of Spin Frustration in a Vanadium Diselenide Monolayer Magnet. *Adv. Mater.* **2019**, *31*, 1901185.

(15) Perfetti, L.; Loukakos, P. A.; Lisowski, M.; Bovensiepen, U.; Berger, H.; Biermann, S.; Cornaglia, P. S.; Georges, A.; Wolf, M. Time Evolution of the Electronic Structure of $1T-TaS_2$ through the Insulator-Metal Transition. *Phys. Rev. Lett.* **2006**, *97*, 067402.

(16) Hellmann, S.; Rohwer, T.; Kalläne, M.; Hanff, K.; Sohrt, C.; Stange, A.; Carr, A.; Murnane, M. M.; Kapteyn, H. C.; Kipp, L.; Bauer, M.; Rossnagel, K. Time-domain classification of charge-density-wave insulators. *Nat. Commun.* **2012**, *3*, 1069 EP –.

(17) Rohwer, T.; Hellmann, S.; Wiesenmayer, M.; Sohrt, C.; Stange, A.; Slomski, B.; Carr, A.; Liu, Y.; Avila, L. M.; Kallane, M.; Mathias, S.; Kipp, L.; Rossnagel, K.; Bauer, M. Collapse of long-range charge order tracked by time-resolved photoemission at high momenta. *Nature* **2011**, *471*, 490–493.

(18) Petersen, J. C.; Kaiser, S.; Dean, N.; Simoncig, A.; Liu, H. Y.; Cavalieri, A. L.; Cacho, C.; Turcu, I. C. E.; Springate, E.; Frassetto, F.; Poletto, L.; Dhesi, S. S.; Berger, H.; Cavalleri, A. Clocking the Melting Transition of Charge and Lattice Order in $1T$-TaS_2 with Ultrafast Extreme-Ultraviolet Angle-Resolved Photoemission Spectroscopy. *Phys. Rev. Lett.* **2011**, *107*, 177402.

(19) Mathias, S. et al. Self-amplified photo-induced gap quenching in a correlated electron material. *Nat. Commun.* **2016**, *7*, 12902 EP –.

(20) Graf, J.; Jozwiak, C.; Smallwood, C. L.; Eisaki, H.; Kaindl, R. A.; Lee, D.-H.; Lanzara, A. Nodal quasiparticle meltdown in ultrahigh-resolution pump–probe angle-resolved photoemission. *Nat. Phys.* **2011**, *7*, 805 EP –.

(21) Smallwood, C. L.; Hinton, J. P.; Jozwiak, C.; Zhang, W.; Koralek, J. D.; Eisaki, H.; Lee, D.-H.; Orenstein, J.; Lanzara, A. Tracking Cooper Pairs in a Cuprate Superconductor by Ultrafast Angle-Resolved Photoemission. *Science* **2012**, *336*, 1137–1139.

(22) Sohrt, C.; Stange, A.; Bauer, M.; Rossnagel, K. How fast can a Peierls–Mott insulator be melted? *Faraday Discuss.* **2014**, *171*, 243–257.

(23) Perfetti, L.; Loukakos, P. A.; Lisowski, M.; Bovensiepen, U.; Eisaki, H.; Wolf, M. Ultrafast Electron Relaxation in Superconducting $Bi_2Sr_2CaCu_2O_{8+\delta}$ by Time-Resolved Photoelectron Spectroscopy. *Phys. Rev. Lett.* **2007**, *99*, 197001.

(24) Monney, C.; Puppin, M.; Nicholson, C. W.; Hoesch, M.; Chapman, R. T.; Springate, E.; Berger, H.; Magrez, A.; Cacho, C.; Ernstorfer, R.; Wolf, M. Revealing the role of electrons and phonons in the ultrafast recovery of charge density wave correlations in $1T$-$TiSe_2$. *Phys. Rev. B* **2016**, *94*, 165165.

(25) Damascelli, A.; Hussain, Z.; Shen, Z.-X. Ange-resolved photoemission studies of the cuprate superconductors. *Rev. Mod. Phys.* **2003**, *75*, 473.

(26) Ulstrup, S.; Johannsen, J. C.; Crepaldi, A.; Cilento, F.; Zacchigna, M.; Cacho, C.; Chapman, R. T.; Springate, E.; Fromm, F.; Raidel, C.; Seyller, T.; Parmigiani, F.; Grioni, M.; Hofmann, P. Ultrafast electron dynamics in epitaxial graphene investigated with time- and angle-resolved photoemission spectroscopy. *J. Phys.: Condens. Matter* **2015**, *27*, 164206.

(27) Andreatta, F.; Rostami, H.; Čabo, A. G.; Bianchi, M.; Sanders, C. E.; Biswas, D.; Cacho, C.; Jones, A. J. H.; Chapman, R. T.; Springate, E.; King, P. D. C.; Miwa, J. A.; Balatsky, A.; Ulstrup, S.; Hofmann, P. Transient hot electron dynamics in single-layer TaS_2. *Phys. Rev. B* **2019**, *99*, 165421.

(28) Johannsen, J. C.; Ulstrup, S.; Cilento, F.; Crepaldi, A.; Zacchigna, M.; Cacho, C.; Turcu, I. C. E.; Springate, E.; Fromm, F.; Raidel, C.; Seyller, T.; Parmigiani, F.; Grioni, M.; Hofmann, P. Direct View of Hot Carrier Dynamics in Graphene. *Phys. Rev. Lett.* **2013**, *111*, 027403.

(29) Pandey, J.; Soni, A. Electron-phonon interactions and two-phonon modes associated with charge density wave in single crystalline $1T{-}VSe_2$. *Phys. Rev. Research* **2020**, *2*, 033118.

(30) Allen, P. B. Theory of thermal relaxation of electrons in metals. *Phys. Rev. Lett.* **1987**, *59*, 1460–1463.

(31) Cavalleri, A.; Tóth, C.; Siders, C. W.; Squier, J. A.; Ráksi, F.; Forget, P.; Kieffer, J. C. Femtosecond Structural Dynamics in VO_2 during an Ultrafast Solid-Solid Phase Transition. *Phys. Rev. Lett.* **2001**, *87*, 237401.

(32) Cavalleri, A.; Dekorsy, T.; Chong, H. H. W.; Kieffer, J. C.; Schoenlein, R. W. Evidence for a structurally-driven insulator-to-metal transition in VO_2: A view from the ultrafast timescale. *Phys. Rev. B* **2004**, *70*, 161102.

(33) Kübler, C.; Ehrke, H.; Huber, R.; Lopez, R.; Halabica, A.; Haglund, R. F.; Leitenstorfer, A. Coherent Structural Dynamics and Electronic Correlations during an Ultrafast Insulator-to-Metal Phase Transition in VO_2. *Phys. Rev. Lett.* **2007**, *99*, 116401.

(34) Wall, S.; Krenzer, B.; Wippermann, S.; Sanna, S.; Klasing, F.; Hanisch-Blicharski, A.; Kammler, M.; Schmidt, W. G.; Horn-von Hoegen, M. Atomistic Picture of Charge Density Wave Formation at Surfaces. *Phys. Rev. Lett.* **2012**, *109*, 186101.

(35) Sun, Y.; Dai, T.; He, Z.; Zhou, W.; Hu, P.; Li, S.; Wu, S. Memristive phase switching in two-dimensional $1T'$-VSe_2 crystals. *Applied Physics Letters* **2020**, *116*, 033101.

(36) Choi, B. K.; Ulstrup, S.; Gunasekera, S. M.; Kim, J.; Lim, S. Y.; Moreschini, L.; Oh, J. S.; Chun, S.-H.; Jozwiak, C.; Bostwick, A.; Rotenberg, E.; Cheong, H.; Lyo, I.-W.; Mucha-Kruczynski, M.; Chang, Y. J. Visualizing Orbital Content of Electronic Bands in Anisotropic 2D Semiconducting $ReSe_2$. *ACS Nano* **2020**, *14*, 7880–7891.

(37) Frassetto, F.; Cacho, C.; Froud, C. A.; Turcu, I. E.; Villoresi, P.; Bryan, W. A.; Springate, E.; Poletto, L. Single-grating monochromator for extreme-ultraviolet ultrashort pulses. *Opt. Express* **2011**, *19*, 19169–19181.

(38) Haule, K.; Yee, C.-H.; Kim, K. Dynamical mean-field theory within the full-potential methods: Electronic structure of $CeIrIn_5$, $CeCoIn_5$, and $CeRhIn_5$. *Phys. Rev. B* **2010**, *81*, 195107.

(39) Blaha, P.; Schwarz, K.; Tran, F.; Laskowski, R.; Madsen, G. K. H.; Marks, L. D. WIEN2k: An APW+lo program for calculating the properties of solids. *J. Chem. Phys.* **2020**, *152*, 074101

(40) Anisimov, V. I.; Aryasetiawan, F.; Lichtenstein, A. I. First-principles calculations of the electronic structure and spectra of strongly correlated systems: the LDA+U method. *J. Phys.: Condens. Matter* **1997**, *9*, 767–808.

(41) Gull, E.; Millis, A. J.; Lichtenstein, A. I.; Rubtsov, A. N.; Troyer, M.; Werner, P. Continuous-time Monte Carlo methods for quantum impurity models. *Rev. Mod. Phys.* **2011**, *83*, 349–404.

(42) Werner, P.; Comanac, A.; de' Medici, L.; Troyer, M.; Millis, A. J. Continuous-Time Solver for Quantum Impurity Models. *Phys. Rev. Lett.* **2006**, *97*, 076405.

(43) Haule, K. Quantum Monte Carlo impurity solver for cluster dynamical mean-field theory and electronic structure calculations with adjustable cluster base. *Phys. Rev. B* **2007**, *75*, 155113.

(44) Jarrell, M.; Gubernatis, J. Bayesian inference and the analytic continuation of imaginary-time quantum Monte Carlo data. *Phys. Rep.* **1996**, *269*, 133 – 195.

(45) Perdew, J. P.; Burke, K.; Ernzerhof, M. Generalized Gradient Approximation Made Simple. *Phys. Rev. Lett.* **1996**, *77*, 3865–3868.

(46) Nechaev, I. A.; Jensen, M. F.; Rienks, E. D. L.; Silkin, V. M.; Echenique, P. M.; Chulkov, E. V.; Hofmann, P. Hole dynamics in a two-dimensional spin-orbit coupled electron system: Theoretical and experimental study of the Au(111) surface state. *Phys. Rev. B* **2009**, *80*, 113402.

(47) Ulstrup, S. et al. Ramifications of optical pumping on the interpretation of time-resolved

photoemission experiments on graphene. *J. Electron Spectrosc. Relat. Phenom.* **2015**, *200*, 340–346.